ACS APPLIED MATERIALS & INTERFACES

Research Article

www.acsami.org

Superior CO Catalytic Oxidation on Novel Pt/Clay Nanocomposites

Dharmesh Varade,[†] Hideki Abe,[‡] Yusuke Yamauchi,[‡,§] and Kazutoshi Haraguchi*,[†]

[†]Material Chemistry Laboratory, Kawamura Institute of Chemical Research, 631 Sakado, Sakura, Chiba 285-0078, Japan

[‡]National Institute for Materials Science (NIMS), 1-1 Namiki, Tsukuba, Ibaraki 305-0044, Japan

[§]Precursory Research for Embryonic Science and Technology (PRESTO), Japan Science and Technology Agency (JST), 4-1-8 Honcho, Kawaguchi, Saitama 332-0012, Japan

Supporting Information

ABSTRACT: Nanostructured novel Pt/Clay nanocomposites consisting of well-defined Pt nanoparticles prepared by clay-mediated in situ reduction displays very high thermal stability, large BET surface area and superior catalytic activity for CO oxidation as compared to a model reference Pt/SiO_2 catalysts. CO oxidation has attracted renewed attention because of its technological importance in the area of pollution control. The Pt/Clay system consisting of Pt nanoparticles strongly immobilized between the atomic layers of clay inhibits nanoparticle sintering and loss of catalytic activity even after prolonged heating at high temperatures. At elevated temperatures (300 °C), the Pt/Clay system demonstrates significant enhancement of catalytic activity, with almost 100% CO conversion in less than 5 min. Emphasis is given to the role played by the clay supporting material which is chemically and thermally stable under the catalytic conditions of exhaust purification.

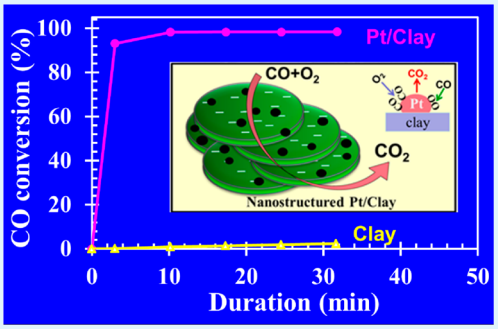

KEYWORDS: *nanocomposites, clay, CO oxidation, exhaust purification, platinum*

INTRODUCTION

Supported precious metal catalysts such as the platinum (Pt)−rhodium (Rh)−palladium (Pd) have been usually employed in several industrial applications,[1−4] especially as automotive three-way catalysts to mitigate harmful gas emissions from gasoline-powered engines.[5−8] Nanoparticle size is well recognized as one of the indispensable factors determining the activity and selectivity of supported nanocatalysts.[9,10] At elevated operation temperatures, the catalyst performance varies markedly with nanoparticle coarsening (decrease in the overall surface area), often leading to catalyst deactivation.[7−10] Similarly, inclusion of organic dispersants may have undesirable consequences such as decreased activity and/or the occurrence of organic residues.[11] To abate these undesirable effects, it is necessary to design well-defined nanoparticle catalysts evenly dispersed on a steady support in the absence of any organic moiety. On the other hand, noble metals are very sparse resources, and hence, their usage as active sites should be reduced to the maximum possible extent for automotive catalysts.

Clay is a low-cost inorganic mineral with a layered structure and has attracted boundless interest as a functional material because of its attractive properties such as ordered structure, intercalation ability, network formation, and high exchange capacity.[12−17] Clay-stabilized nanoparticles have been synthesized in some cases.[18−22] Recently, we reported a novel synthetic route to versatile Pt/Clay system via clay-mediated in situ reduction under mild conditions, without using any organic modifiers.[23,24] Moreover, the Pt/Clay features a very large surface area, high stability, and outstanding catalytic activity, and is hence considered appropriate for varied prospective applications, for example, as a cutting-edge nanocatalyst. Considering the growth of the present automobile society, there is a strong demand for the production of advanced automotive catalysts with high activity and increased longevity, designed with the minimal use of precious metals, so that they can meet the upcoming highly stringent emission restrictions. In this context, the core objective of the present study was to explore the prospective applications of this nanostructured Pt/Clay hybrid system with focus on its catalytic activity for carbon monoxide (CO) oxidation, which is an important reaction for both industrial and automotive pollution control.[25] The catalytic activity of the Pt/Clay system in the CO oxidation reaction was compared to the Pt/SiO_2 model catalyst[4] system to make the process more viable for practical uses.

EXPERIMENTAL SECTION

Materials. The inorganic clay, "synthetic hectorite: Laponite XLG" ($[Mg_{5.34}Li_{0.66}Si_8O_{20}(OH)_4]Na_{0.66}$ with a cation-exchange capacity of 104 mequiv/100 g; Rockwood, Ltd., UK) was used after being purified, washed, and vacuum-dried. SiO_2 (particle size 20−200 nm) was obtained from C. I. Kasei Co. Ltd. Analytical-grade potassium tetrachloroplatinate (II) (K_2PtCl_4) was purchased from Wako Pure Chemical Industries, Japan. Ultrapure water supplied by a PURIC-MX system (Organo Co., Japan) was used for all experiments.

Received: July 24, 2013
Accepted: October 21, 2013
Published: October 21, 2013

Preparation of Clay-Supported Pt Nanoparticles. Clay dispersion was prepared by swelling the clay (0.2 g) in deionized water (10 g) at 40 °C for 60 min. To the resulting dispersion (1 wt %) was added aged K_2PtCl_4 solution (500 μL; 5 wt %) with continuous stirring for 2 min. The mixed solutions containing clay and Pt species were maintained in the dark under static conditions at room temperature (25 ± 1 °C). The formation of Pt nanoparticles was indicated by the color change of the reaction solution from light brown-yellow to opaque black within 24 h of mixing. After the removal of water, the residue was dried for 2 h at 80 °C.

Preparation of SiO_2-Supported Pt Nanoparticles. The detailed experimental procedure for preparing the Pt/SiO_2 materials is described elsewhere.[3] Aqueous H_2PtCl_6 solution (292.6 mL; 0.3 wt %) was added gently to aqueous polyvinylpyrrolidone (300 mL; 22.5 mmol). After stirring, ethanol (150 mL) was added to the solution, followed by reflux at 100 °C for 6 h. The yellow precursor solution turned black during reflux. It was then distilled under reduced pressure to yield a black solution. The concentration of Pt in the Pt nanoparticle solution was determined to be 0.62 wt % by Inductively Coupled Plasma (ICP) analysis. Three portions of Pt nanoparticles (0.25, 0.50, and 1.0 wt %) relative to the amount of SiO_2 were added to 20 g of a SiO_2 suspension in 200 mL of deionized water. Upon the removal of water, the residue was dried for 2 h at 120 °C. The final product was crushed and then calcined at 450 °C in air for 2 h to yield the desired catalysts.

Characterization. The morphology of the nanoparticles was examined using a high-resolution field-emission transmission electron microscope (JEM-2200TFE, JEOL) operating at 200 kV. Energy-dispersive X-ray spectroscopy (EDS) was performed using scanning transmission electron microscopy (STEM) with a JEOL JEM-2200TFE instrument operating at 200 kV. XRD patterns were obtained using a Rigaku SmartLab X-ray diffractometer with monochromatic Cu Kα radiation (40 kV, 100 mA). The final dry Pt/Clay material was crushed then calcined at 300 and 500 °C in air to yield the desired material. Nitrogen adsorption–desorption data were obtained using a BELSORP-mini II (BEL JAPAN Inc.) operated at 77 K. The CO oxidation reaction was performed over the catalyst in a circulating-gas reactor equipped with a gas chromatograph (Shimadzu GC-8A). The catalyst was vacuum-dried in the reactor at 200 °C prior to the reaction. A mixture of CO (6.67 kPa) and O_2 (3.33 kPa) was then circulated through the catalyst at different temperatures. The formation of CO_2 was monitored at each temperature by gas chromatography. Temperature-programmed desorption (TPD) of CO was performed using a vacuum chamber (back pressure <1 mPa) equipped with a quadrupole mass spectrometer (QMAS; Qulee YTP-50M, ULVAC). A sample mass of 100 mg was thoroughly dried in the vacuum chamber at 400 K for 12 h, and was subjected to 10 kPa of CO gas at 300 K for 10 min. The sample temperature was then raised from 300 to 450 at 10 K min^{-1}, whereas the CO concentration in the vacuum chamber was continuously monitored with the QMAS.

RESULTS AND DISCUSSION

In the preparation of the Pt/Clay system, the inorganic clay mineral smectite (e.g., synthetic hectorite: Laponite XLG) acts as a mild and effective reducing agent for K_2PtCl_4 (Pt(II) ions) and as an outstanding stabilizer of the resulting Pt nanoparticles, which likely occurs via successive proton–electron transfer processes as described below

$$2SiOH + PtCl_2 \rightarrow SiOSi + Pt + 2HCl \quad (1)$$

Figure 1a shows the photograph of the as-prepared Pt/Clay system (Pt loading 0.25 wt %) in the powdered state. The representative TEM image displayed in Figure 1b and the corresponding energy-dispersive X-ray spectroscopy (EDS) mapping of the Pt (inset; Figure 1b) clearly show the well-defined, small Pt nanoparticles (3–6 nm) formed in the clay dispersion, adhering to the disklike clay platelets (30 nm in diameter, with a thickness of 1 nm).[26] In the present study, we

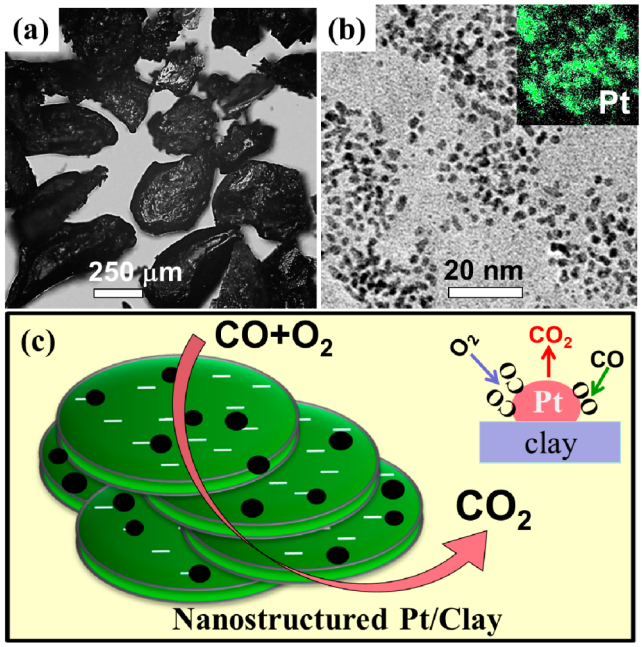

Figure 1. (a) Photograph of dried Pt/Clay system prepared in clay dispersion (10 g; 1 wt %) containing K_2PtCl_4 (500 μL; 5 wt %). (b) TEM image and inset showing the corresponding energy-dispersive X-ray spectroscopy (EDS) mapping for Pt. (c) Schematic representation of Pt/Clay system for CO oxidation reaction.

investigated the intriguing catalytic activity of this Pt/Clay system in the carbon monoxide (CO) oxidation reaction. It is well-known that CO oxidation on Pt proceeds via a Langmuir–Hinshelwood reaction,[6] as illustrated in Figure 1c.

The catalytic activities of the Pt/Clay system and Pt/SiO_2 reference system with identical Pt loading (0.25 wt %) were investigated at various elevated temperatures (150, 175, 200, and 300 °C) in the oxidation of CO by oxygen (O_2). Pt/SiO_2 system have gained particular attention as a prototype system and as active catalysts in the CO oxidation reaction.[3,27] The results are shown in Figure 2a (Pt/Clay) and Figure 2b (Pt/SiO_2) respectively. In both cases, the reaction was performed under same conditions using 6.67 kPa CO and 3.33 kPa O_2. Time courses of CO conversion indicate that the activity of the Pt/Clay system was inferior to that of Pt/SiO_2 in CO oxidation below 175 °C. The CO conversion rate of Pt/Clay was lesser than one-half that of Pt/SiO_2 at any duration. However, there was a substantial increase in the catalytic activity of the Pt/Clay system at elevated temperatures. For example, at 200 °C, Pt/Clay exhibited a higher CO conversion rate (almost 80% after 30 min) at any duration, relative to CO conversion rate (only 60% after 30 min) for Pt/SiO_2. More importantly, at 300 °C, significant enhancement of the catalytic activity (nearly a 10-fold increase) was observed with almost 100% CO conversion in less than 5 min, which is an important and novel characteristic of this unique Pt/Clay system. On the other hand, at 300 °C, the Pt/SiO_2 system displayed moderately lower activity; hardly 10% CO conversion in 5 min.

Pt/Clay system calcined in air at 300 °C exhibit almost similar activity to those of as-prepared one (data not shown). Moreover, the catalytic activity of the Pt/Clay material calcined at 500 °C in air for 2 h, demonstrates the further improved activity under analogous conditions, as shown in Figure 2c. For example, at 200 °C, noteworthy enhancement of the catalytic activity (nearly a 2-fold increase) was observed with essentially

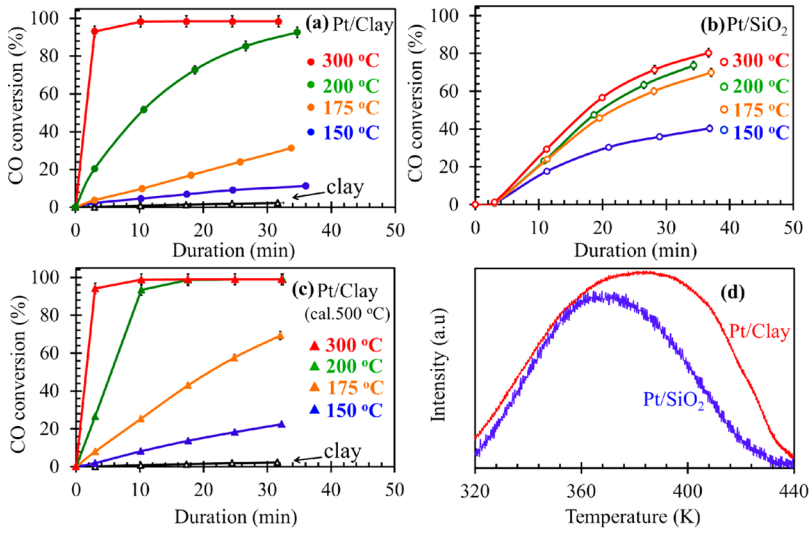

Figure 2. CO oxidation at various temperatures using (a) as-prepared Pt/Clay system, (b) as-prepared Pt/SiO_2, and (c) Pt/Clay calcined at 500 °C for 2 h, (d) CO-temperature-programmed desorption (TPD) profiles for Pt/SiO_2 (blue), and Pt/clay (red). Control experiments conducted on clay (without Pt) for CO oxidation reaction are indicated in (a), and (c).

100% CO_2 production, which surpasses even to that reported for Pt_3Ti/SiO_2 (Pt-based intermetallic compound) at corresponding temperature.[3] At 300 °C, 100% CO conversion was also observed in less than 5 min. These demonstrate the excellent thermal stability and very high activity of the Pt/Clay system even after calcination. Furthermore, the effect of Pt loading on the CO conversion efficiency depicted in Figure S1 in the Supporting Information indicate that a Pt loading amount as low as 0.05 wt % is enough to induce superior catalytic activity at 300 °C. Besides, the fact that the control experiments conducted on clay (without Pt) showed virtually no CO_2 production (see Figure 2) indicates that CO conversion is entirely because of the in situ formed ultrasmall Pt nanoparticles. Thus, it is deduced that the nanostructured Pt/Clay system has great potential for use as a nanocatalyst for exhaust purification.

We performed CO-temperature-programmed desorption (TPD) analysis to further understand the catalytic properties of Pt/Clay and Pt/SiO_2 as depicted in Figure 2d. A peak at 370 K on the CO-TPD profile for Pt/SiO_2 was identified, corresponding to the thermal desorption of CO molecules from the surface of the supported Pt nanoparticles, which is consistent with the reported light-off temperature of the CO oxidation reaction over the surface of pure Pt.[6] In contrast, the CO-TPD profile for Pt/Clay showed a very broad peak consisting of a continuous distribution of different peaks ranging from 370 to 400 K. The peaks distributed above 370 K were ascribed to the CO desorption from the clay-embedded Pt nanoparticles situated away from the edge of the clay platelets, suggesting that a larger distance between the platelet edge and the Pt nanoparticles requires a longer time for the escape of desorbed CO molecules into the atmosphere, resulting in a delayed response to CO desorption and a broadening in the CO-TPD peak. The apparently low CO conversion activity of Pt/Clay at low temperatures is attributed to sluggish migration of CO molecules through the interatomic layers of the clay. Note that the CO-TPD profiles for both Pt/Clay and Pt/SiO_2 decreased steeply at temperatures higher than 420 K and converged to a background level when the temperature reached 440 K, showing that the CO migration in the atomic layers of clay became as fast as that over Pt/SiO_2 at high temperatures. Indeed, Pt/Clay exhibited a more superior CO conversion activity to Pt/SiO_2 at temperatures higher than 200 °C (473 K), because of the promoted CO migration and suppressed agglomeration of Pt nanoparticles. It is rational to conclude that the reaction kinetics over the Pt nanoparticles in Pt/Clay is the same (Langmuir–Hinshelwood type) as that over Pt/SiO_2 and pure Pt surfaces, because the intrinsic CO-desorption temperatures for Pt/SiO_2 and Pt/Clay were identical within experimental errors, as well as consistent with the reported light-off temperature for pure Pt surfaces.

The large difference in the catalytic activity with comparable particle sizes between Pt/Clay (see Figure 1b) and Pt/SiO_2 systems (see Figure S2a in Supporting Information) cannot be attributed to particle size effects. The reason for this distinct behavior might be related to the divergent properties of the underlying substrate as discussed above. Moreover, hydroxyl groups have indeed been reported to be part of the active sites and have triggered oxygen activation on Au catalysts supported on "inert" oxides such as alumina[28,29] and silica.[30] However, in this study, both Pt/Clay and Pt/SiO_2 catalysts were preheated at 200 °C before testing the CO conversion activity. This preheating step at high temperatures nullifies any possible influence from the hydroxyl groups as these groups are lost at temperatures above 175 °C due to dehydroxylation.[29] From the BET surface areas of the catalysts determined using N_2 adsorption–desorption isotherms (Figure 3 and Table 1), it is evident that the Pt/Clay catalyst has a higher surface area and a smaller pore size compared to those of the Pt/SiO_2 catalyst. Furthermore, the surface coverage of the adsorbed CO and oxygen is always higher in the Pt/Clay catalyst compared to that observed with the Pt/SiO_2 catalyst. Hence the catalyst surface is essentially poisoned by adsorbed CO at low temperatures. However, there is a sudden increase in the CO conversion at ~200 °C (light-off temperature). This is because at higher temperatures, CO begins to desorb from the catalyst surface, creating more free sites available for oxygen to dissociate. Because oxygen dissociates rapidly, CO_2 is produced quickly.

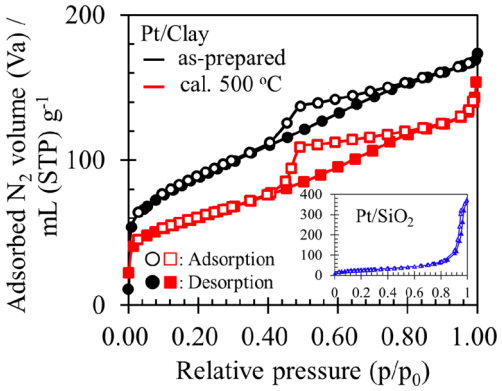

Figure 3. N_2 adsorption–desorption isotherm for Pt/Clay catalyst as-prepared (black) and calcined at 500 °C (red). Inset shows the N_2 adsorption–desorption isotherm for Pt/SiO_2.

Table 1. N_2 Adsorption–Desorption Analysis of the Catalysts

catalysts	BET surface area (m^2 g^{-1})	avg pore size (nm)
clay	314	4.4
Pt/clay (as-prepared)	312	4.2
Pt/clay (cal. 500 °C)	215	5.0
Pt/SiO_2	90	24.3

To confirm the stability of the Pt/Clay system, we have performed X-ray diffraction (XRD) and transmission electron microscopy (TEM) analyses. Figure 4 shows the TEM images with corresponding histograms (calculated from randomly selected 100 nanoparticles) of the Pt/Clay system (a) as-prepared, and calcined at (b) 300 °C and (c) 500 °C in air for 2 h. Interestingly, neither the size of the nanoparticles nor their distribution alter significantly upon calcination at 300 °C (Figure 4b), highlighting the outstanding stability and ultralow mobility of the Pt nanoparticles in the Pt/Clay system. However, a minor sintering effect was detected subsequently upon increasing the calcination temperature to 500 °C (Figure 4c): a final average size of 4–8 nm was reached. Nevertheless, the high catalytic activity and large surface area of the Pt/Clay system was still reserved. On the contrary, the SiO_2 support itself is unstable even at 300 °C leading to change in the material characteristics (see Figure S2b in the Supporting Information). Additional TEM images of the Pt/Clay system (Pt loading 0.05 wt %) calcined at 300 and 500 °C, which display high thermal stability, are also shown in Figure S3 in the Supporting Information.

The corresponding XRD measurements of the neat clay (without Pt), as-prepared Pt/Clay system, and those after calcination at 300 and 500 °C in air for 2 h are illustrated in Figure 5a. The XRD pattern for the neat clay and as-prepared

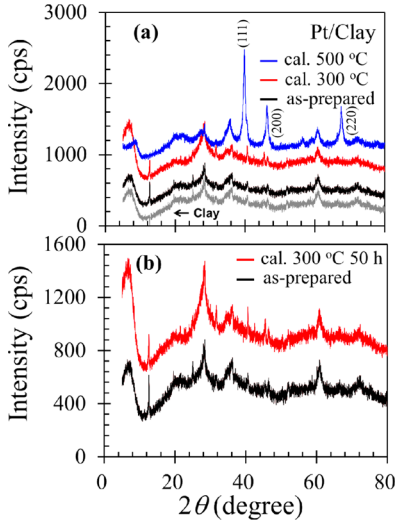

Figure 5. XRD measurements presented for (a) clay, Pt/Clay as-prepared, and calcined in air at 300 and 500 °C for 2 h. The diffraction peaks for Pt are indexed. (b) Pt/Clay as-prepared and calcined in air at 300 °C for 50 h.

Pt/Clay is almost identical demonstrating no change in the clay structure even after the clay-mediated in situ formation of Pt nanoparticles. XRD pattern for the as-prepared Pt/Clay showed

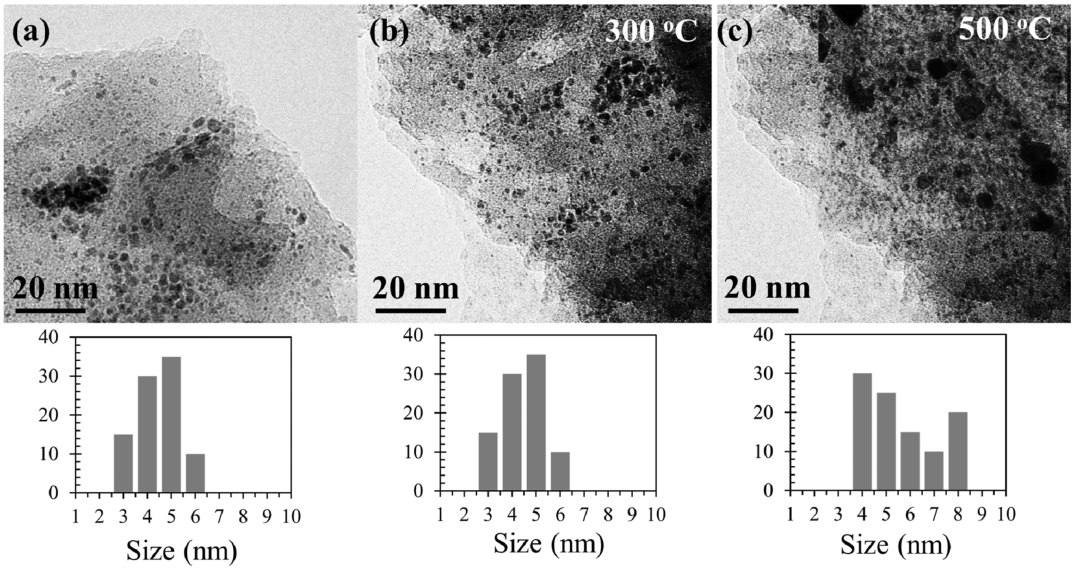

Figure 4. TEM images and the corresponding particle size distribution of Pt/Clay system (a) as-prepared, and after calcination at (b) 300, and (c) 500 °C for 2 h.

no crystalline peaks for the Pt nanoparticles, probably because of the very small particle size.[31] Furthermore, the XRD spectrum was unchanged upon subsequent calcination at 300 °C indicating absolutely intact structure. However, data revealed small but sharp signals for crystalline Pt after calcination at 500 °C, attributable to the minor growth of the particles owing to their coarsening, which is consistent with the TEM observation. The diffraction peaks for Pt can be assigned to the (111), (200), and (220) Miller indices of the standard face-centered structure. Interestingly, Figure 5b indicates that the Pt/Clay structure is highly robust under the reaction conditions for CO oxidation, as shown by the virtually identical XRD spectra, even after prolonged calcination at 300 °C for 50 h. This observation is particularly important for aforementioned application because the Pt/Clay demonstrated superior catalytic activity around this temperature. This is also consistent with the thermogravimetric (TG) analysis (see Figure S4 in the Supporting Information) of the as-prepared Pt/Clay material, in which no characteristic decomposition or evaporation peaks were observed over this temperature range.

The most critical problem associated with industrial catalysts is thermal agglomeration of the catalytic centers at high temperatures, which greatly degrades catalytic performance. The Pt/Clay system studied here is most probably free from substantial thermal agglomeration, because the nanoparticles were strongly immobilized between the atomic layers of clay. Furthermore, the Pt/Clay system retained its high CO oxidation activity even after calcination at elevated temperatures, which is indicative of its excellent stability. These preliminary results undoubtedly specify that Pt/Clay hybrid system has great potential for use as a high-temperature catalyst, in terms of the improved agglomeration tolerance.

CONCLUSIONS

The current study opens a more efficient and extremely versatile pathway to implementing large-surface area Pt/Clay systems as an effective nanocatalyst for the purification of automobile exhaust in terms of their superior catalytic activity toward CO oxidation at relatively low Pt content compared with the conventional Pt/SiO_2 catalyst. We strongly believe that our results will be of general interest well beyond the presented system and that a complete understanding of this apparently simple reaction could serve as a platform to explore other selective oxidation reactions. Furthermore, the proposed study would certainly help in crafting more rational approaches to develop better functional automobile catalysts using clay mineral supports.

ASSOCIATED CONTENT

Supporting Information

TGA measurements, additional TEM images, and Co conversion data. This material is available free of charge via the Internet at http://pubs.acs.org.

AUTHOR INFORMATION

Corresponding Author

*E-mail: hara@kicr.or.jp.

Notes

The authors declare no competing financial interest.

ACKNOWLEDGMENTS

This work was supported by the Ministry of Education, Science, Sports and Culture of Japan (Grant-in-Aid 23350117). The authors thank DIC analysis center (DIC Corp.) for the TEM and XRD measurements.

REFERENCES

(1) Norskov, J. K.; Bligaard, T.; Rossmeisl, J.; Christensen, C. H. *Nat. Chem.* **2009**, *1*, 37−46.
(2) Chen, A.; Holt-Hindle, P. *Chem. Rev.* **2010**, *110*, 3767−3804.
(3) Saravanan, G.; Abe, H.; Xu, Y.; Sekido, N.; Hirata, H.; Matsumoto, S.; Yoshikawa, H.; Yamabe-Mitarai, Y. *Langmuir* **2010**, *26*, 11446−11451.
(4) Behafarid, F.; Rolden Cuenya, B. *Nano Lett.* **2011**, *11*, 5290−5296.
(5) Heck, R. M.; Farrauto, R. J.; Gulati, S. T. *Catalytic Air Pollution Control*; Van Nostrand Reinhold: New York, 2009.
(6) Bowker, M. *Chem. Soc. Rev.* **2008**, *37*, 2204−2211.
(7) Nishihata, Y.; Mizuki, J.; Akao, T.; Tanaka, H.; Uenishi, M.; Kimura, M.; Okamoto, T.; Hamadak, N. *Nature* **2002**, *418*, 164−167.
(8) Nagai, Y. *R&D Rev. Toyota CRDL* **2011**, *42*, 43−50.
(9) Naitabdi, A.; Behafarid, F.; Roldan Cuenya, B. *Appl. Phys. Lett.* **2009**, *94*, 083102−3.
(10) Mostafa, S.; Behafarid, F.; Croy, J. R.; Ono, L. K.; Li, L.; Yang, J. C.; Frenkel, A. I.; Roldan Cuenya, B. *J. Am. Chem. Soc.* **2010**, *132*, 15714−15719.
(11) Leontyev, I. N.; Belenov, S. V.; Guterman, V. E.; Haghi-Ashtiani, P.; Shaganov, A. P.; Dkhil, B. *J. Phys. Chem. C* **2011**, *115*, 5429−5434.
(12) Hu, N. F.; Rusling, J. F. *Anal. Chem.* **1991**, *63*, 2163−2168.
(13) Macha, S. M.; Fitch, A. *Mikrochim. Acta* **1998**, *128*, 1−18.
(14) Zhou, Y. L.; Li, Z.; Hu, N. F.; Zeng, Y. H.; Rusling, J. F. *Langmuir* **2002**, *18*, 8573−8579.
(15) Van Olphen, H. *An Introduction to Clay Colloid Chemistry*, 2nd ed.; Wiley-Blackwell: New York, 1977.
(16) Haraguchi, K.; Ebato, M.; Takehisa, T. *Adv. Mater.* **2006**, *18*, 2250−2254.
(17) Haraguchi, K.; Takehisa, T. *Adv. Mater.* **2002**, *14*, 1120−1124.
(18) Datta, K. K. R.; Kulkarni, C.; Eswaramoorthy, M. *Chem. Commun.* **2010**, *46*, 616−618.
(19) Zhang, R.; Hummelgard, M.; Olin, H. *Langmuir* **2010**, *26*, 5823−5828.
(20) Burridge, K.; Johnston, J.; Borrmann, T. *J. Mater. Chem.* **2011**, *21*, 734−742.
(21) Abdullayev, E.; Sakakibara, K.; Okamoto, K.; Wei, W.; Ariga, K.; Lvov, Y. *ACS Appl. Mater. Interfaces* **2011**, *3*, 4040−4046.
(22) Varadwaj, G. B. V.; Parida, K. M. *RSC Adv.* **2013**, *3*, 13583−13593.
(23) Varade, D.; Haraguchi, K. *Langmuir* **2013**, *29*, 1977−1984.
(24) Varade, D.; Haraguchi, K. *Phys. Chem. Chem. Phys.* **2013**, *15*, 16477−16480.
(25) Bielamnski, A.; Haber, J. *Oxygen in Catalysis*; Marcel Dekker: New York, 1991.
(26) Haraguchi, K.; Li, H. J.; Matsuda, K.; Takehisa, T.; Elliot, E. *Macromolecules* **2005**, *38*, 3482−3490.
(27) McClure, S. M.; Lundwall, M.; Zhou, Z.; Yang, F.; Goodman, D. W. *Catal. Lett.* **2009**, *133*, 298−306.
(28) Centeno, M. A.; Hadjivanov, K.; Venkov, T.; Klimev, H.; Odriozola, J. A. *J. Mol. Catal. A: Chem.* **2006**, *252*, 142−149.
(29) Ivanova, S.; Pitchon, V.; Petit, C.; Caps, V. *ChemCatChem* **2010**, *2*, 556−563.
(30) Gajan, D.; Guillois, K.; Delichere, P.; Basset, J.-M.; Candy, J.-P.; Caps, V.; Coperet, C.; Lesage, A.; Emsley, L. *J. Am. Chem. Soc.* **2009**, *131*, 14667−14669.
(31) Pina-Zapardiel, R.; Montero, I.; Esteban-Cubillo, A.; Moya, J. S.; Kaplan, W. D.; Paramasivam, T.; Pecharroman, C. *J. Nanopart. Res.* **2011**, *13*, 5239−5249.